Mon. Not. R. Astron. Soc. **311**, 565–575 (2000)

Hubble Space Telescope imaging of the CFRS and LDSS redshift surveys – IV. Influence of mergers in the evolution of faint field galaxies from $z \sim 1$

O. Le Fèvre,[1★] R. Abraham,[2] S. J. Lilly,[3] R. S. Ellis,[2] J. Brinchmann,[2] D. Schade,[6] L. Tresse,[1,4] M. Colless,[5] D. Crampton,[6] K. Glazebrook,[7] F. Hammer[8] and T. Broadhurst[9]

[1]*Laboratoire d'Astronomie Spatiale - CNRS, Traverse du Siphon, B.P.8, 13376 Marseille Cedex 12, France*
[2]*Institute of Astronomy, University of Cambridge, Madingley Road, Cambridge CB3 0HA*
[3]*Department of Astronomy, University of Toronto, 60 St George Street, Toronto, Ontario, M5S 3H8, Canada*
[4]*Istituto di Radioastronomia – CNR, Via P. Gobetti, 101 40129 Bologna, Italy*
[5]*Mount Stromlo & Siding Spring Observatories, Australian National University, Weston Creek, Canberra, ACT 2611, Australia*
[6]*Dominion Astrophysical Observatory, 5071 West Saanich Road, Victoria, BC, V8X 4M6, Canada*
[7]*Anglo-Australian Observatory, P.O. Box 296, Epping, NSW 1710, Australia*
[8]*DAEC, Observatoire de Paris-Meudon, 92195 Meudon Cedex, France*
[9]*Department of Astronomy, University of California, 601 Campbell Hall, University of California, Berkeley CA 94720-3411, USA*

Accepted 1999 September 1. Received 1999 September 1; in original form 1998 August 12

ABSTRACT

Hubble Space Telescope images of a sample of 285 galaxies with measured redshifts from the Canada–France Redshift Survey (CFRS) and Autofib–Low Dispersion Spectrograph Survey (LDSS) redshift surveys are analysed to derive the evolution of the merger fraction out to redshifts $z \sim 1$. We have performed visual and machine-based merger identifications, as well as counts of bright pairs of galaxies with magnitude differences $\delta m \leq 1.5$ mag. We find that the pair fraction increases with redshift, with up to ~20 per cent of the galaxies being in physical pairs at $z \sim 0.75$–1. We derive a merger fraction varying with redshift as $\propto (1+z)^{3.2\pm0.6}$, after correction for line-of-sight contamination, in excellent agreement with the merger fraction derived from the visual classification of mergers for which $m = 3.4 \pm 0.6$. After correcting for seeing effects on the ground-based selection of survey galaxies, we conclude that the pair fraction evolves as $\propto (1+z)^{2.7\pm0.6}$. This implies that an average L^* galaxy will have undergone 0.8–1.8 merger events from $z = 1$ to $z = 0$, with 0.5 to 1.2 merger events occuring in a 2-Gyr time-span at around $z \sim 0.9$. This result is consistent with predictions from semi-analytical models of galaxy formation. From the simple coaddition of the observed luminosities of the galaxies in pairs, physical mergers are computed to lead to a brightening of 0.5 mag for each pair on average, and a boost in star formation rate of a factor of 2, as derived from the average [O II] equivalent widths. Mergers of galaxies are therefore contributing significantly to the evolution of both the luminosity function and luminosity density of the Universe out to $z \sim 1$.

Key words: galaxies: evolution – galaxies: interactions – cosmology: observations.

1 INTRODUCTION

Mergers of galaxies have long been known to play an important role in the evolution of galaxies. Detailed case studies in the local Universe have shown the powerful effect mergers can have on galaxy morphologies and on the triggering of star formation (eg. Kennicutt 1996; Schweizer 1996). The importance of mergers has also been emphasized by computer simulations involving either major mergers of galaxies with comparable mass, or the merger of dwarf galaxies with a more massive galaxy (Mihos & Hernquist 1994a,b; Hernquist & Mihos 1995; Mihos 1995, hereafter M95).

If merging is at work at all during the lifetime of galaxies, then the space density, mass, luminosity, and morphology of galaxies must change with epoch. Several authors suggest that merging systems can explain part (or all) of the excess number of galaxies observed in deep photometric galaxy counts (Rocca-Volmerange & Guiderdoni 1990; Broadhurst, Ellis & Glazebrook 1992). Mergers can influence such surveys either by the separate counting of individual systems ultimately destined to merge, or through more subtle effects. For example, dissipative mergers are expected to trigger some degree of star formation, so in

★ E-mail: lefevre@astrsp-mrs.fr

magnitude-limited samples one expects to observe less massive galaxies brightened above observational limits by merger-induced star formation activity.

The evolution of the merger rate with redshift is a key observable that can be used to test galaxy formation models (see Abraham 1998 for a review). In particular, semi-analytical models for galaxy formation in hierarchical clustering scenarios postulate that galaxies assemble from the successive merger of smaller subunits. Such models make concrete predictions for the relationships between evolution in the morphological mix and redshift-dependent merger rates (Baugh et al. 1996, 1998; Kauffmann, White & Guiderdoni 1993; Kauffmann 1996).

Evolution of the luminosity function of galaxies at high redshifts (Lilly et al. 1995; Ellis et al. 1996) indicates that, on the whole, either the typical luminosity of galaxies was brighter by $\sim$1 magnitude at $z \sim 0.7$, or that there were $\sim$3 times more galaxies at this epoch, or that a combination of both luminosity and number density evolution is occurring. Disentangling the effects of these two phenomena is central to understanding the nature of field galaxy evolution. Luminosity evolution has been shown to play an important role in the evolution of disc galaxies, from observations with the *Hubble Space Telescope* (*HST*) of systems from the CFRS–LDSS sample (Schade et al. 1995; Lilly et al. 1998). On the other hand, number-density evolution remains poorly constrained.

There are several reasons why meaningful constraints on number-density evolution have been difficult to obtain. One needs large galaxy samples with redshifts measured up to large look-back times *and* deep high spatial resolution images in order to observe the close environment of galaxies at better than 1 kpc resolution. Furthermore, the time-scales associated with merging are not straightforward to constrain. There is considerable uncertainty in any transformation from an 'instantaneous' merger rate (computed directly from observations at a given look-back time) to a 'global' merger rate indicating the likelihood for a galaxy to experience merging from any epoch to the present.

Data from the *HST* indicates that, at moderate redshifts, there is a larger proportion of faint galaxies exhibiting peculiar morphologies suggestive of merging (Griffiths et al. 1994; Driver et al. 1995; Glazebrook et al. 1995; Neuschaefer et al. 1997). Following early attempts to measure the evolution of the merger fraction (Zepf & Koo 1989), these *HST* observations complement studies of close pairs of galaxies from redshift survey samples (Carlberg, Pritchet & Infante 1994; Yee & Ellingson 1995; Woods, Fahlman & Richer 1995; Patton et al. 1997) out to intermediate redshifts $z \sim 0.3$. In a pair study of a complete sample of galaxies with measured redshifts, Patton et al. (1997) find that at a mean redshift $z \sim 0.33$, 4.7 ± 0.9 per cent of galaxies are in close physical pairs, compared with 2.1 ± 0.2 per cent locally (Patton et al. 1997), leading to a change in the merger rate with redshift proportional to $(1+z)^{2.8\pm0.9}$.

The CFRS (Lilly et al. 1995; Le Fèvre et al. 1995) and LDSS surveys (Colless et al. 1993; Glazebrook et al. 1995) provide samples with several hundred galaxies with redshifts measured up to $z \sim 1.2$. Well-defined subsamples from these surveys have been observed with the *HST*, allowing us to obtain quantitative information on the morphological type mix (Brinchmann et al. 1998), the central disc and bulge surface brightnesses (Lilly et al. 1998; Schade et al., 1999), and, in the present paper, the close environment of the survey galaxies and the merger rate as a function of redshift.

In the present paper we present the measurements of the merging rate of galaxies out to redshifts $\sim$1, from *HST* cycle 4 and cycle 5 imaging of a total sample of 285 galaxies. The paper is organized as follows. Our sample is described in Section 2. Visual identifications of merging galaxies, as well as pair counts based on both visual and computer-based classifications, are presented in Section 3. The evolution of the merger rate out to $z \sim 1$ is computed in Section 4, and the luminosity enhancement and selection effects introduced by mergers on the magnitude limited sample are evaluated in Section 5. A discussion of the results is presented in Section 6. We use $H_0 = 50\,\mathrm{km\,s^{-1}\,Mpc^{-1}}$ and $q_0 = 0.5$ throughout this paper.

2 HST IMAGING SAMPLE

Imaging data was primarily acquired during *HST* cycles 4 and 5 with the Wide Field and Planetary Camera 2 (WFPC2) and the F814W filter. In addition, field CFRS 1415+52 [set on a deep Very Large Array (VLA) field; Fomalont et al. 1991] was observed with the *HST* as part of the 'Groth strip' campaign (Groth et al. 1994), and was included in the present data set. Exposure times varied between 4400 and 7400 s, and allowed us to reach signal-to-noise ratios of $S/N = 1$ per WFPC2 pixel for $\mu_{I_{AB}} = 25.3\,\mathrm{mag\,arcsec^{-2}}$. This surface brightness limit is deep enough to trace an unevolved Milky Way-like disc to three scalelengths at the redshift limit of our combined survey. The full CFRS + LDSS *HST* imaging data set is described in detail in Brinchmann et al. (1998). A total of 232 CFRS galaxies and 53 Autofib + LDSS galaxies have both a securely measured redshift in the range $0.05 \leq z \leq 1.2$ (with a redshift identification secure at the 85 per cent level: Le Fèvre et al. 1995; Brinchmann et al. 1998, table II), and a deep *HST*/WFPC2 image. Galaxies in the CFRS are drawn from a purely *I*-band selected sample, as defined in Lilly et al. (1995) and Le Fèvre et al. (1995). Galaxies in the LDSS sample are a purely *B*-selected sample, as defined in Colless et al. (1993) and Glazebrook et al. (1995). Galaxies near the edge of the WFPC2 field (those systems for which a full $20\,h^{-1}$ kpc area around them was not visible) were removed from the sample. The redshift and magnitude distributions of the *HST* samples are similar to the distributions of their parent CFRS and LDSS samples (as described by Brinchmann et al. 1998).

3 IMAGE ANALYSIS

3.1 Visual identification of mergers

In this section we seek to identify merger events through visual classification. In this procedure we attempt to distinguish broadly between probable 'major' and 'minor' merging events. A major merger, involving galaxies of comparable masses, should produce strong morphological signatures, such as double nuclei, wisps, tails, shells, asymmetric morphology, and possibly be associated with the triggering of a recent starburst (Mihos & Hernquist 1994; Liu & Kennicutt 1995). Minor mergers, involving a massive galaxy and a small dwarf, are likely to be more frequent (M95; Baugh et al. 1996), and produce more benign morphological signatures, which might be difficult to identify during or shortly after the merging event, although significant changes of the star formation rate can result from this type of event. It is emphasized that the visibility of merger-induced features may be relatively short-lived, depending on the respective masses of the galaxies involved (M95), making the identification of even relatively recently completed mergers a challenging task.

We have defined the following visual classification scheme to identify merger events:

(0) not a merger: no trace of merger, although some minor asymmetry may be present.

(1) suspicious: there is a suspicion that some merging event might be occurring, with some asymmetry and traces of wisps, tails, etc.

(2) probable merger/upcoming merger: there is a nearby galaxy but the isophotes are not overlapping at the $\mu_{I_{AB}} = 25.3\,\mathrm{mag\,arcsec^{-2}}$ isophote level.

(3) on-going merger: a merging event is most probably or certainly occurring, as evidenced by strong asymmetry, double nuclei, prominent wisps, tails, etc.

In the following analysis, classes 2 and 3 are summed to produce the list of visually identified mergers. The separation in classes 2 and 3 is used in Section 5.2, but we emphasize that the separation between classes 2 and 3 is sensitive to the depth of the limiting isophote chosen, as the primary and companion galaxy may well be 'bridged' by luminous material at levels fainter than the observations are able to reveal.

All galaxies in the sample have been visually examined by three of us (JB, OLF, SJL), and classified in the above scheme. When a classification was discrepant among the three observers, the median class has been taken as the final classification. A total of 261 galaxies have a secure redshift measurement; among these, 22 are classified in class 3, and four in class 2. This leads to an overall merger fraction for the whole sample of 10 ± 2 per cent. A total of 63 galaxies do not have a redshift, of which three are in class 2 and four are in class 3, giving a merger fraction for this sample of 11 ± 4 per cent. Galaxies without redshifts therefore have a merger fraction comparable to that for the whole sample, and no bias in the merger-rate estimate is expected from restricting the analysis to galaxies with secure redshifts. The list of visually identified mergers is given in Table 1. Images of the mergers are presented in Fig. 1 and the histogram of the redshift distribution is shown in Fig. 2. The fraction of visually identified mergers versus redshift is shown in Fig. 2: it is evident that most of the identified mergers are at the high-redshift end of the sample.

Table 1. List of visually identified mergers. I_{AB} and $M_B(AB)$ are the *I*-band and absolute blue magnitudes in the *AB* reference system; EW(O II) is the rest-frame [O II]3727 equivalent width. See Section 3.1 for the definition of the merger class.

Num	Redshift z	I_{AB} Ground	$M_B(AB)$	Rest EW(O II)	Merger Class
03.0523	0.6508	21.31	−21.19	30.3	3
03.1540	0.6898	21.04	−21.51	11.8	3
10.0761	0.9832	22.07	−21.55	8.1	3
10.0765	0.5365	22.18	−19.95	52.7	3
10.0802	0.3090	21.70	−19.16	32.9	3
10.1183	0.6487	20.60	−21.92	34.6	3
10.1220	0.9092	22.36	−20.95	20.4	2
14.0377	0.2596	20.81	−19.61	62.7	3
14.0485	0.6545	22.16	−22.44	35.7	2
14.0547	1.1600	21.40	−23.09	6.0	3
14.0665	0.8090	22.97	−20.78	12.2	2
14.0743	0.9860	22.19	−22.05	14.1	2
14.0846	0.9890	21.81	−21.91	40.9	3
14.1126	0.7426	22.26	−20.64	41.9	3
14.1129	0.8310	21.12	−22.10	15.3	3
14.1139	0.6600	20.20	−22.27	12.0	3
14.1415	0.7450	21.06	−21.62	0.	3
22.0497	0.4705	18.42	−22.93	0.	3
22.0576	0.8905	22.29	−20.97	73.5	3
22.0599	0.8891	21.74	−21.51	68.8	3
22.0919	0.4738	21.77	−20.23	10.2	3
22.1313	0.8191	21.74	−21.33	57.2	3
22.1453	0.8164	21.44	−21.53	0.	3
10.12073	0.4920	20.35	−20.61	0.	3
13.12106	0.5560	21.70	−18.68	9.0	3
13.12545	0.8300	20.30	−21.26	24.0	3

3.2 Pair fraction

Another approach to identifying mergers is to count pairs of galaxies as observed in projection, and to use these pair counts to estimate the physical pair fraction in the sample (see e.g. Patton et al. 1997). Physical pairs of galaxies separated by small distances and with low relative speeds are bound and are destined to merge on relatively short time-scales. We have performed a pair-count analysis using both a visual approach (based on counts of galaxies with measured redshifts for which nearby galaxies form a pair as observed in projection), and using the machine-based automated approach described in Section 3.2.2. Because we usually have knowledge of the redshift for only one of the pair components, some of the pairs can be produced by foreground–background projection contamination. This effect needs to be corrected for in order to estimate physical pair counts, which can then be related to the merger rate. This section describes the manual and automated classification methods used to estimate the apparent pair fraction, leading to the computation of the physical pair fraction in the next section.

3.2.1 Visual identification of galaxy pairs

We have determined pair counts based on galaxies with at least one nearby companion galaxy within a $20\,h^{-1}$ kpc radius, and a magnitude difference $\delta m \leq 1.5$ mag between the main galaxy and the companion. Such systems are expected to merge within less than $\sim 10^9$ yr (M95; Patton et al. 1997). The difference in magnitude is intended to identify unambigous pairs, and to produce pair counts less affected by the difficulties inherent in separating minor mergers of dwarf galaxies with bright galaxies from galaxies with large H II regions or asymmetric features. These minor mergers can certainly contribute to the general evolution of the morphology and luminosity of galaxies, but the corresponding pair counts are subject to larger uncertainties than the bright pair counts, because of possible significant background contamination. The $\Delta m \leq 1.5$ mag cut-off therefore leads to an underestimate of the true pair fraction.

The visual measurements were carried out as follows. For each galaxy in the CFRS–LDSS catalogue with an *HST*/WFPC2 image, we measured the projected distances $d_1,\ldots,\ d_i$ to putative companion galaxies, and their corresponding magnitude differences $\delta m_1,\ldots,\ \delta m_i$ with respect to the primary galaxy. Objects sharing a common isophote with the primary galaxy were noted in an attempt to broadly distinguish between 'upcoming' and 'ongoing' mergers (see Section 5.2). Galaxy pairs were flagged as '1' when the separation

$$d_\theta = \frac{c}{H_0}\frac{q_0 z + (q_0 - 1) \times (-1 + (1 + 2q_0 z)^{0.5}}{q_0^2 \times (1+z)^2}$$

between the primary galaxy and the companion was less than $20\,h^{-1}$ kpc, and the magnitude difference δm_i was less than 1.5 mag.

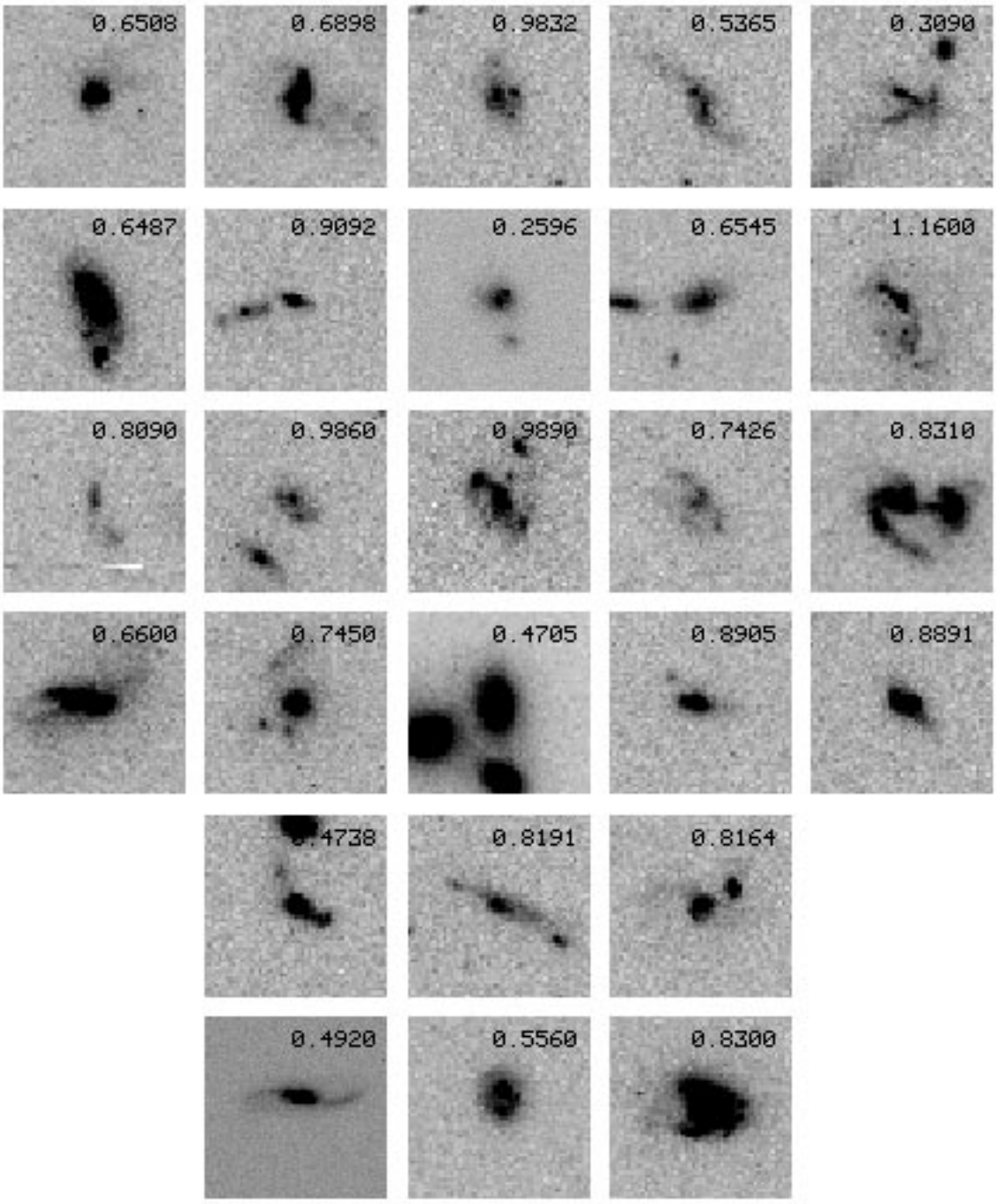

Figure 1. Galaxies visually classified as mergers. Each individual image is 5×5 arcsec^2, the measured redshift is indicated on the upper right corner of each image.

3.2.2 Automated identification of pairs: Lee classifier

In addition to the visual approach defined above, we have undertaken the measurement of a quantitative parameter indicative of merging. The degree of bimodality in the galaxy images is determined objectively from measurements of the Lee ratio (Abraham 1998), $L_{\rm R}$, for each of the galaxy images. Our definition of $L_{\rm R}$ is a straightforward generalization of the maximum-likelihood statistic developed by Fitchett & Webster (1987) for use with sparsely sampled galaxy cluster data (see also Lee 1979). Sky-subtracted 100×100 pixel 'postage stamp' images were constructed for each galaxy in the sample, and the galaxian light isolated from the sky background at the 2σ level. The galaxian-light distribution $I_{i,j}$ at pixel i,j in each of these images was then projected on to a line at angle θ, defining a profile $P(r|\theta)$, where r is the distance along the axis of projection:

$$P(r|\theta) = \sum_{i=-50}^{50} \sum_{j=-50}^{50} I_{i,j} \delta(r - i\cos\theta - j\sin\theta).$$

For each projection, a function L was determined by subdividing

the projection at a number of cuts:

$$L(d|\theta) = \frac{(\mu_l - \mu)^2 + (\mu_r - \mu)^2}{\sigma_l + \sigma_r},$$

where d is the position of the cut, μ_l and σ_l (μ_r and σ_r) are the mean and standard deviations of the profile to the left (right) of the cut, and μ is the mean of the original profile, i.e.

$$\mu_l(d|\theta) = \sum_{w=-50}^{d} wP(w|\theta)$$

$$\mu_r(d|\theta) = \sum_{w=d}^{50} wP(w|\theta)$$

$$\mu(\theta) = \sum_{w=-50}^{50} wP(w|\theta)$$

$$\sigma_l(d|\theta) = \sum_{w=-50}^{d} (w - \mu_l)^2 P(w|\theta)$$

$$\sigma_r(d|\theta) = \sum_{w=d}^{50} (w - \mu_r)^2 P(w|\theta).$$

The Lee ratio L_R is then defined as the ratio of the maximum to the minimum of the L for all angles and all cuts:

$$L_R = \frac{\max_{-50<d<50}^{0<\theta<\pi} L(d|\theta)}{\min_{-50<d<50}^{0<\theta<\pi} L(d|\theta)}.$$

L_R was calibrated using images of synthetic 'mergers' constructed by adding together distinct galaxy images with a range of relative brightnesses and displaced across a range of separations spanning the range observed in the *HST* image sample (Abraham et al. 1998). L_R was computed in steps of 5 degrees. L_R is most sensitive to cases where the magnitude difference between two galaxies is small, and where the isophotes between primary and companion galaxies are overlapping. The L_R parameter is therefore sensitive only to *major* mergers. Values of $L_R > 1.5$ are indicative of significant bimodality.

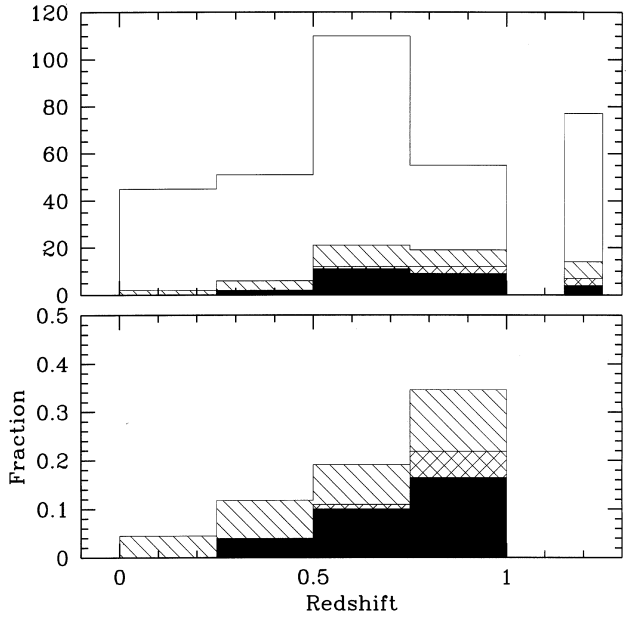

Figure 2. Numbers (*top panel*) and fraction of galaxies (*bottom panel*) visually classified as mergers. The ongoing mergers (class 3, see text) are identified as the filled histogram, probable mergers are identified as the double crossed histogram (class 2), and suspicious galaxies are identified by the single crossed histogram (class 1). The top panel shows as a separate histogram (right) the distribution in classes for the galaxies without redshift.

3.2.3 *Comparison of manual and automated classifications*

A comparison between manually and automatically classified ($L_R \geq 1.5$) pairs of galaxy images was made. Of the 49 pairs identified by the manual approach, 37 (80 per cent) have a Lee ratio $L_R \geq 1.5$. The remaining 12 galaxies were examined in detail, and it was found that of these the manual classification had picked out 10 systems with well-defined bimodal components, while two galaxies with low L_R were wrongly classified as mergers during the manual classification. The majority of bimodal systems not flagged as such by L_R were found to have been rejected because of the 2σ isophote cut imposed on the data fed into the Lee classification program – at this level a few weakly bridged systems were split into individual objects, which separately have low Lee ratios. Lowering the isophote limit to the level used for the manual classification in Section 3.2.1 recovered most of the same pairs identified in the manual classification. In addition, a total of 37 galaxy images (of 285) have $L_R \geq 1.5$ but were not classified as major mergers through the visual classification scheme. Most of these were not classified as pairs either because the magnitude difference between the components of the pairs was $\delta m \geq 1.5$, or because there was a companion galaxy, but outside of the $r = 20\,h^{-1}$ kpc area, or because a bright unresolved object (presumably a star) was nearby. The manual and the L_R classifications are therefore broadly consistent.

In Fig. 3, the L_R parameter for all galaxies in the sample is presented, and the 49 galaxies manually classified as pairs are

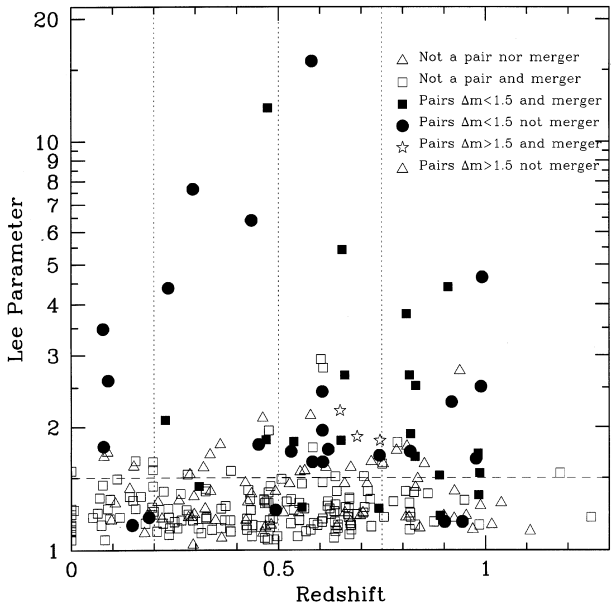

Figure 3. Lee paremeter versus redshift. Symbols used for the different categories of galaxies are identified in the upper right corner.

identified. This comparison leads to the final list of pairs reported in Table 2, and to the images shown in Fig. 4.

3.2.4 Comparison between visually identified mergers and galaxy pairs

Among galaxies visually classified as mergers, 21 galaxies are also classified as pairs, and five galaxies are not (galaxy numbers 10.1183, 14.377, 14.0547, 14.1415, 10.12073). These five galaxies exhibit signs of asymmetry, faint wisps, or tails – leading to the merger classification – but without double nuclei or close companions. The remaining systems all exhibit double nuclei or close companions, and warrant classification as pairs.

3.2.5 Physical pair fraction

The identification of pairs in our images is based on projected appearance. Because in essentially all cases only the redshift of the brightest galaxy is available from our ground-based surveys, we need to correct the number of observed pairs for the appearance of non-physical pairs originating in background/foreground contamination along the line of sight, before we can

Table 2. List of identified pairs. L_R is the Lee ratio, A the asymmetry of the light distribution as defined in Abraham (1998), δm and d are the magnitude difference and the distance in arcsec and kpc between the two galaxies in the pair, respectively. A value '9999' indicates that L_R or A could not be computed.

Num	z	I_{AB} Ground	$M_{AB}B$	L_R	A	Rest EW(O II)	δm	d arcsec/kpc
(1)	(2)	(3)	(4)	(5)	(6)	(7)	(8)	(9)
3.0332	0.1880	21.88	−17.63	1.2	0.323	6.7	1.39	0.55/2.2
3.0466	0.5304	22.47	−19.60	1.74	0.208	20.3	0.65	1.95/14.2
3.0485	0.6056	22.22	−20.24	2.44	9999	66.6	0.80	0.40/3.1
3.0488	0.6069	21.58	−20.85	1.64	9999	67.8	0.50	0.56/4.3
3.0523	0.6508	21.31	−21.19	1.85	0.362	30.3	1.38	0.35/2.7
3.0595	0.6061	21.46	−20.78	1.96	9999	17.4	1.40	0.15/1.1
3.1056	0.9440	22.33	−21.10	1.17	0.23	46.3	1.20	2.3/19.5
3.1319	0.6200	21.51	−20.67	1.76	0.071	25,9	1.50	0.50/3.9
3.1540	0.6898	21.04	−21.51	1.89	0.133	11.8	1.45	1.81/14.4
10.0761	0.9832	22.07	−21.55	1.36	0.005	8.07	1.40	0.44/3.7
10.0765	0.5365	22.18	−19.95	1.84	0.128	52.7	0.23	0.61/4.5
10.0794	0.5800	21.55	−20.53	15.73	0.212	0.	0.24	1.50/11.3
10.0802	0.3090	21.70	−19.16	1.43	0.172	32.9	1.00	1.8/10.1
10.0805	0.1475	21.45	−17.51	1.15	9999	0.	−0.08	4.4/14.8
10.1168	1.1592	22.22	−21.99	9999	9999	103.3	0.10	0.77/6.6
10.1220	0.9092	22.36	−20.95	4.40	0.09	20.43	0.46	1.43/12.0
10.1643	0.2345	20.77	−18.93	4.38	0.177	0.	−0.81	3.84/18.1
10.1644	0.0767	19.56	−17.24	3.48	0.220	0.05	0.81	3.84/7.6
14.0485	0.6540	22.16	−20.44	5.42	0.089	35.7	0.35	2.3/18.0
14.0600	1.0385	21.53	−22.16	9999	9999	26.5	1.26	0.21/1.8
14.0665	0.8090	22.41	−20.65	3.78	0.233	−9	0.36	1.12/9.2
14.0725	0.5820	22.32	−19.76	1.64	0.213	31.0	1.50	0.55/4.1
14.0743	0.9860	21.65	−21.93	1.54	0.131	−9	−0.14	1.83/15.6
14.0749	0.8180	22.45	−20.53	1.74	0.207	−9	0.33	0.39/3.2
14.0846	0.9820	21.81	−21.79	1.72	0.276	40.9	1.49	0.85/7.2
14.0854	0.9920	21.50	−22.21	4.65	0.06	0.	1.31	2.18/18.1
14.0939	0.9180	21.20	−22.15	2.30	0.219	−9	0.49	1.35/11.4
14.1079	0.9011	21.95	−21.35	1.17	0.106	25.2	0.68	0.40/3.4
14.1126	0.7426	22.26	−20.64	1.26	0.109	41.9	0.95	0.20/1.6
14.1129	0.8310	21.05	−22.01	2.52	0.310	−9	0.26	0.81/6.7
14.1139	0.6600	20.20	−22.27	2.68	0.279	12.0	0.62	0.55/4.3
14.1146	0.7437	21.72	−21.06	1.70	0.210	39.0	1.32	0.51/4.1
14.1193	0.0780	21.48	−16.66	1.79	0.279	0.	0.50	1.20/2.4
14.1264	0.7030	22.90	−19.96	9999	9999	−9	0.02	2.02/16.1
14.1501	0.9890	21.74	−21.85	2.51	0.324	−9	0.03	0.65/5.5
22.0497	0.4700	18.42	−22.93	1.86	9999	0.	−0.25	2.16/14.9
22.0576	0.8910	22.29	−20.97	1.21	0.302	73.5	0.50	0.50/4.2
22.0585	0.2940	20.59	−19.46	7.65	0.053	0.	0.45	2.41/13.1
22.0599	0.8890	21.74	−21.51	1.52	0.439	68.8	0.10	0.10/0.8
22.0919	0.4740	21.77	−20.23	12.08	0.268	10.2	0.07	2.25/15.7
22.0953	0.9770	22.27	−21.22	1.67	0.063	47.5	1.30	0.70/6.0
22.1313	0.8190	21.74	−21.33	1.92	0.202	57.2	1.47	1.97/16.4
22.1453	0.8160	21.44	−21.53	2.68	0.076	0.	0.34	1.08/9.0
10.12525	0.4350	20.00	−21.35	6.40	9999	2.1	0.67	2.55/17.1
13.12106	0.5560	21.70	−18.68	1.27	0.132	9.0	1.47	0.60/4.4
13.12111	0.0890	22.60	−14.40	2.60	0.260	37.7	1.10	4.4/9.8
13.12540	0.4520	22.60	−17.61	1.81	9999	0	0.75	0.50/3.4
13.12545	0.8300	20.30	−21.26	1.69	0.396	24.0	0.01	0.60/5.0
13.12549	0.4930	21.10	−18.88	1.25	0.052	8.7	0.79	2.80/19.8

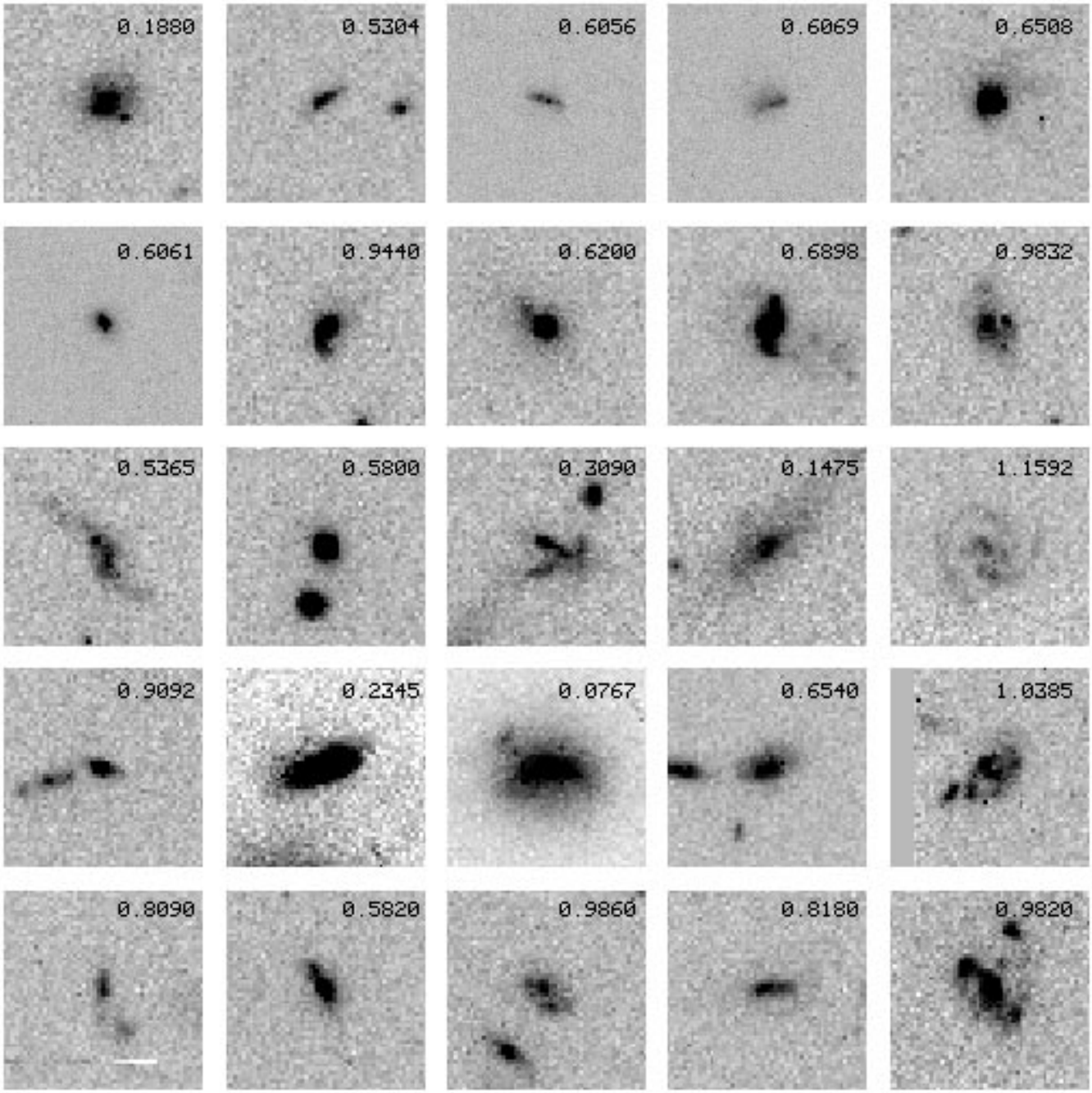

Figure 4. Galaxies classified as pairs. Each individual image is 5×5 arcsec^2, the measured redshift is indicated on the upper right corner of each image

obtain an estimate of the true number of physical pairs. The background/foreground contamination correction was calculated using the counts published by Driver et al. (1995) and Abraham et al. (1996), integrated over the magnitude range $m_{\rm main} < m_{\rm gal} < m_{\rm main} + 1.5$ and within a projected $20\,h^{-1}$ kpc radius area. At $z \sim 1$, the limiting magnitude $I_{AB} = 24.5$ of the *HST* images allows us to securely identify all galaxies brighter than $M_B = -17.5$. For each galaxy, this M_B was then used with the K-correction $k(z)$ of the primary galaxy to compute the apparent magnitude down to which the counts were to be performed, and the background/foreground contamination applied. It is noteworthy that the detailed form of the K-correction has only a minor effect on this calculation, because the observed I-band corresponds to rest B-band at $z \sim 0.9$.

Our results are summarized in Table 3, which lists the numbers of galaxies, observed pairs, and expected line-of-sight contamination. The pair fraction reported in Table 3 has been computed as the fraction of pairs in the sample, corrected for the expected number of non-physical projected pairs. The statistics of our survey are such that the pair fraction can be measured with good precision for the highest two redshift bins, while at $z < 0.5$ the numbers of pairs are smaller and the background/foreground contamination is higher because $20\,h^{-1}$ kpc projects to a larger projected angular area.

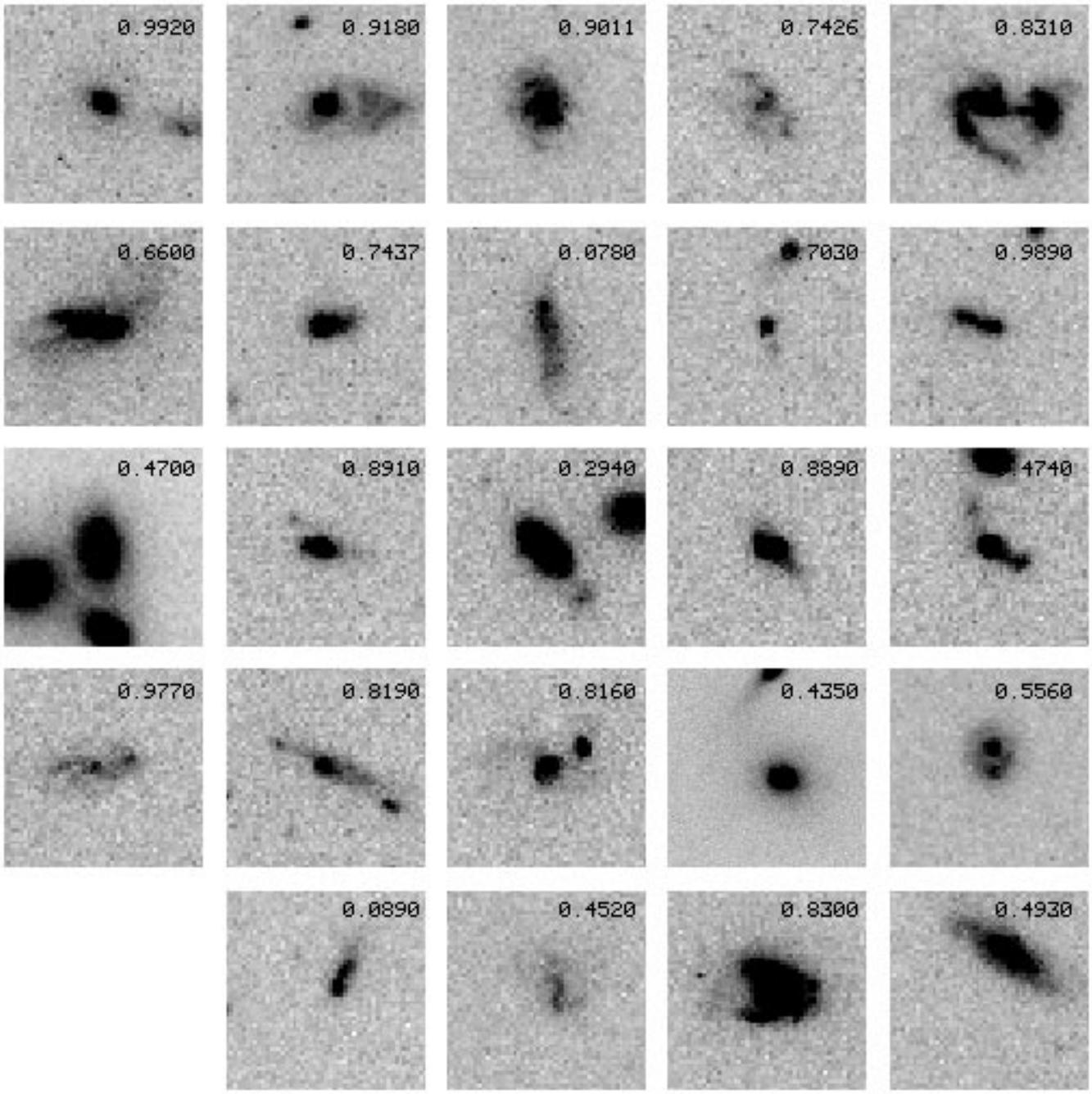

Figure 4 – *continued*

4 EVOLUTION OF THE MERGER RATE

Our data allow us to determine the first direct observational measurement of the merger fraction at redshifts $z > 0.5$. We can derive the merger fraction from both (complementary) approaches that we have followed. Within the current sample, both the fraction of mergers and the pair fraction rise by a factor of more than 2 between redshifts 0.5 and 0.9. Compared with local measurements of the merger fraction (Patton et al. 1997), the merger fraction at $z \sim 0.9$ is more than nine times higher than in the local universe.

From the visual classification of mergers, we find that the merger fraction is 5.8 ± 2.6, 10.5 ± 3.5, 21.8 ± 6.3 per cent, at mean redshifts 0.37, 0.63 and 0.9, respectively. If we take the local merger value to be 2.1 ± 0.2 per cent (Patton et al. 1997), a least-squares fit of this data gives, for the evolution of the merger fraction parametrized as $R_{\rm merg}(z) = R_{\rm merg}(0) \times (1+z)^m$, $R_{\rm merg}(0) = 0.021 \pm 0.004$ and $m = 3.4 \pm 0.6$. Our redshift $z = 0.37$ result is compatible with the merging fraction of 4.7 ± 0.9 per cent at $z = 0.33$ from Patton et al. (1997).

Our pair counts (corrected for background/foreground contamination) indicate that at redshifts $z = 0.63$ and $z = 0.91$, 9.9 ± 3.5 and 20.3 ± 5.7 per cent of the galaxy pairs are likely to be physical, respectively. However, as pointed out by Carlberg et al. (1994) and Patton et al. (1997), one needs to determine the fraction of these physical pairs that are likely to merge. Patton et al. (1997) suggest

that, at the present epoch, 50 per cent of the galaxy pairs with relative velocities less than 350 km s^{-1} are likely to merge. This is expected to change with redshift as $(1+z)^{-1}$. Applying this correction, we find that the merger fractions at $z = 0.63$ and $z = 0.91$ are 8.1 ± 3.3 and 19.4 ± 5.7 per cent, respectively. Using all of the four CFRS–LDSS *HST* data points in Table 3 in combination with the lower-redshift measurement of 4.7 ± 0.9 per cent at $z = 0.33$, and a local merging fraction of 2.1 ± 0.2 per cent (Patton et al. 1997), we find that the pair-count-estimated merger fraction evolves as $(1+z)^{3.2\pm0.6}$, in excellent agreement with the merger fraction from the morphological criteria. The data points are represented in Fig. 5. To minimize the impact of the apparent magnitude selection on our sample, which selects predominantly low luminosity galaxies at low redshifts and high luminosity galaxies at high redshifts, we have repeated the above analysis, limiting our sample to galaxies with $M_{B_{AB}} \geq 20.5$. We find that at redshifts $z = 0.65$ and $z = 0.906$, 7.8 ± 4.1 and 21.0 ± 6.1 per cent of the galaxy pairs are physical pairs likely to merge. Using our four data points and the data from Patton et al., we find that the best fit is $R_{\rm merg}(0) = 0.019 \pm 0.004$ and $m = 3.25 \pm 0.63$.

Therefore, using both visually identified mergers and pair counts, we conclude that the observed merger rate evolves with redshifts as $(1+z)^m$ with m ranging from 3.2 to 3.4, over the redshift range 0–1.

5 LUMINOSITY ENHANCEMENT FROM MERGERS

Mergers can change the luminosity function of galaxies through a combination of both number density and luminosity evolution. In

Table 3. Pair fraction. $N_{\rm gal}$, $N_{\rm maj}$ and $N_{\rm proj}$ are the total number of galaxies in each sample bin, the number of galaxies classified as major mergers, and the expected background and foreground galaxy contamination. The pair fraction is $N_{\rm maj} - N_{\rm proj}/N_{\rm gal}$; multiplied by $0.5(1+z)$ provides the expected physical pair fraction.

Sample	z	$N_{\rm gal}$	$N_{\rm maj}$	$N_{\rm proj}$	Pair Fraction	Pair Fraction corr. $0.5(1+z)$
All CFRS+LDSS	0–0.2	40	6	22	0	0
All CFRS+LDSS	0.2–0.5	98	11	19	0	0
All CFRS+LDSS	0.5–0.75	89	21	12.2	9.9	8.1
All CFRS+LDSS	0.75–1.3	62	21	8.4	20.3	19.4
CFRS+LDSS $M_{B_{AB}} \leq -20.5$	0–0.2	8	0	7.1	0	0
CFRS+LDSS $M_{B_{AB}} \leq -20.5$	0.2–0.5	33	2	4.3	0	0
CFRS+LDSS $M_{B_{AB}} \leq -20.5$	0.5–0.75	57	12	6.6	9.5	7.8
CFRS+LDSS $M_{B_{AB}} \leq -20.5$	0.75–1.3	59	21	8.0	22.0	21.0

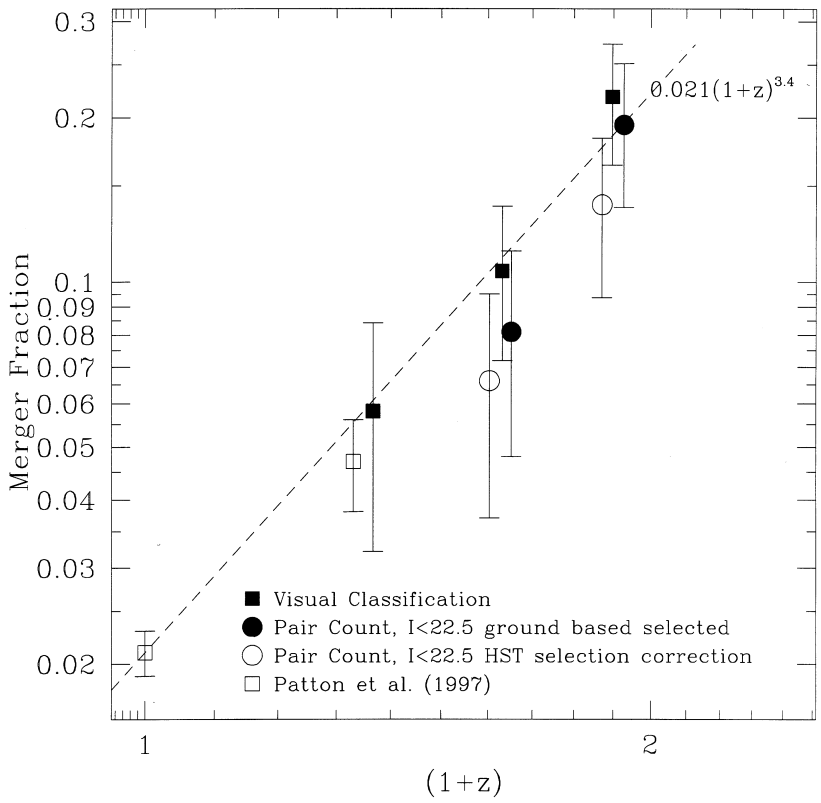

Figure 5. Evolution of the fraction of visually confirmed mergers (filled squares) and of the physical pair fraction (filled circles). The physical pair fraction corrected from the smearing effect present in a ground-based magnitude selected sample is presented as open circles (see Section 6). The empty squares are from Patton et al. (1997). The different points at $z = 0.63$ and $z = 0.91$ have been slightly shifted in the plot for clarity.

addition to the obvious effects of density evolution, mergers may also brighten galaxies to the point where systems that would otherwise drop below the magnitude limits of a survey become included in the sample.

Two effects can contribute to the luminosity enhancement of a galaxy in a merging pair. In a dissipationless merger, the luminosities of the two galaxies add with a final luminosity being (at most) twice that of the most luminous pre-merging galaxy. However, merging may also trigger additional stellar formation, particularly during later stages of the merging process (Hernquist & Mihos 1995), increasing the total luminosity by adding to the overall stellar content of the combined system. As star formation activity should have a longer time-scale than the time-scale during which the morphological evidence for a merger remains (M95), a global star formation increase might be expected in a galaxy population subjected to a higher rate of merging. These two effects are quantified in the following sections.

5.1 Luminosity brightening

The brightening of the galaxy population induced by merging can be one of the contributors to the observed evolution of the luminosity function (Lilly et al. 1995; Ellis et al. 1996). To estimate the brightening of the population from merging, we looked at the brightest pairs selected from our $\delta m \leq 1.5$ mag criterion. The minimum luminosity enhancement induced by a close pair, if destined to merge, has simply been taken as the coaddition of the luminosities of the galaxies in a pair, assuming no extra star formation triggered by the event. We have computed the magnitudes of each galaxy in a pair from the *HST* images (excluding close companions) and a conservative estimate of the final magnitude of the merged pair was obtained by simply adding the luminosities from the two galaxies, the resulting magnitude being equal to the ground-based magnitude (Brinchmann et al. 1998). The luminosity enhancement estimated by this simple procedure is shown in column 8 of Table 2 for each pair, and is on average 0.5 mag for the sample of galaxies classified as pairs. There are 37 pairs above $z = 0.5$, of which 19 are expected to be the result of projection effects. This indicates that 18/151 galaxies, or $\sim 11.9 \pm 2.8$ per cent of the galaxies at $z \geq 0.5$ will experience a brightening of at least 0.5 mag within the next billion years or so due to merging. As the merger time-scales are subject to considerable uncertainties, we can only speculate that this fraction of galaxies is the minimum fraction of galaxies in the sample that would experience a brightening over a time-span of ~ 2 Gyr. We note that some of these galaxies will be brought artificially into a magnitude-limited sample produced from ground-based observations, because the total magnitude of the galaxy is coming from closely paired galaxies as the result of projection effects (Table 3), with each of the individual galaxies in the pair being fainter than the magnitude limit of the sample, as described in Section 6.

5.2 Star formation rate increase

To estimate the star formation enhancement produced during the merger process, we have looked at the [O II]3727 Å equivalent width for three subsamples: ongoing mergers, upcoming mergers, and galaxies with no companions, as classified during the analysis detailed in Section 3.2.1. *Ongoing major mergers*, have been defined as systems with evidence for double nuclei within $20\,h^{-1}$ kpc, each galaxy having comparable luminosity ($\leq$1.5 mag), sometimes associated with disrupted morphologies. *Upcoming* major mergers are defined as systems with a galaxy with $\delta m \leq 1.5$ mag at a distance $d \leq 20\,h^{-1}$ kpc from a galaxy in the redshift sample, but where the isophotes of the two galaxies are not overlapping at the depth of our images. Of course, a single galaxy can have a total number of upcoming or ongoing mergers larger than one. Differences in the [O II] equivalent width between the ongoing and upcoming merger classes could then indicate the effect of merging on the star formation rate.

Our results are summarized in Table 4, which shows that the [O II] equivalent width of upcoming mergers is not significantly different from the equivalent width of non-merging galaxies, while the equivalent width of ongoing mergers at $z \geq 0.5$ is >38 Å, 2 times higher than for non-merger galaxies (~ 19 Å). Ongoing mergers may thus have a star formation rate increased by a factor of 2, with a corresponding luminosity increase, as a result of the merging process. It is noteworthy that a significant fraction of the star formation may be obscured by dust, as dust is often seen in merging systems, and therefore, that the star formation rate increase measured from [O II] should be taken as a lower limit (Hammer et al. 1997).

6 BIAS IN GROUND-BASED SELECTED SAMPLES FROM MERGER-INDUCED LUMINOSITY ENHANCEMENT

In this section we examine the effect of having selected our galaxy sample from a redshift survey based on ground-based imaging. Some of the galaxies in the redshift survey are now identified from the *HST* imaging as pairs of nearby galaxies, unresolved in ground-based data. Seeing effects clearly lead ground-based surveys to include some galaxies in magnitude-limited samples only because the added luminosity from a close companion is sufficient to produce a total blended luminosity above a limiting magnitude threshold. From the analysis of the magnitude difference with the closest companion as described in Section 5.1, we find that in the galaxies of the CFRS sample imaged with *HST*, 11 (of 232) galaxies have been included in the ground-based redshift survey because of this effect. This is most significant for $z > 0.7$, as 6 (of 73) galaxies above this redshift are in the complete *HST*-CFRS sample because of this effect, which enters at the 8 ± 3 per cent level. This bias also demonstrates the difficulties inherent in comparing deep galaxy counts obtained from ground-based and space-based observations.

Taking this effect into account would lower the physical pair fraction, corrected for background/foreground contamination, from 9.9 to 8.1 per cent at $z = 0.63$ and from 20.3 to 14.5 per cent at $z = 0.91$. This would lower the parameter m describing the physical pair rate change with redshift to $m = 2.7 \pm 0.6$.

7 DISCUSSION AND CONCLUSION

The visual classification of mergers, and the pair-count analysis performed using manual classifications and using the Lee

Table 4. Rest-frame [O II] equivalent width for major mergers

z	Upcoming mergers	$N_{\rm gal}$	Ongoing mergers	$N_{\rm gal}$	Other galaxies	$N_{\rm gal}$
< 0.5	8.3	11	2.7	5	12.6	123
0.5–0.75	15.0	7	37.7	15	18.9	67
> 0.75	24.8	5	46.4	9	19.7	48

classifier, paint a consistent picture of the effects of mergers on high-redshift galaxies. Our analysis shows that major mergers of galaxies ($\delta m \leq 1.5$) are playing an increasingly important role at higher redshifts, both in terms of number evolution and in inducing a significant luminosity enhancement. From the visual classification of mergers, we find that the merger fraction evolves as $(1+z)^m$, with $m = 3.4 \pm 0.6$, in excellent agreement with the merger fraction derived from the pair counts, for which $m = 3.2 \pm 0.6$.

As shown explicitly in Section 6, ground-based magnitude-limited imaging samples can be biased by the effects of seeing, as close pairs of galaxies are counted singly. Around ~8 per cent of high redshift $z > 0.7$ galaxies that are formally below the selection limit would be included in a ground-based $I_{AB} \leq 22.5$ mag sample owing to this effect. If our magnitude-limited redshift survey had been defined from *HST* imaging data rather than from imaging data limited by ground-based seeing, the pair fraction at $z \sim 0.9$ would be lowered from ~20 to 14.5 per cent. After correction for this bias, we conclude that the merger-fraction evolution exponent can best be parametrized as $m = 2.7 \pm 0.6$.

Transforming the observed merger fraction into a merger rate requires knowledge of the average time-scale over which a merger is completed (i.e. over which morphological traces of the merger are gone at the 1 kpc resolution at which we are observing the present sample). Although there are considerable uncertainties in estimating this time-scale, an upper limit of 400 Myr to 1 Gyr seems reasonable from both data and simulations (e.g. Patton et al. 1997; Mihos & Hernquist 1995). Our results indicate that between redshift 0 and 0.9, the merger probability is $\sim 0.38 \times [(2\,\mathrm{Gyr} \times q_0^{0.5})/\tau]$, where τ is the merger time-scale, and $\sim 0.2 \times [(2\,\mathrm{Gyr} \times q_0^{0.5})/\tau]$ between $z = 0.75$ and $z = 1.2$. Using a (conservative) range of merger timescales from 400 Myr to 1 Gyr, these relations suggest a galaxy will undergo on average 0.8 to 1.8 merger events from $z = 1$ to $z = 0$, with 0.5 to 1.2 merger events occurring in a 2-Gyr time-span at $z \sim 0.9$.

Semi-analytical models of galaxy formation in hierarchical clustering theories make strong predictions regarding the high-redshift merger rate. The model of Baugh et al. (1996) predicts that more than 50 per cent of the elliptical galaxies, and 15 per cent of the spiral galaxies suffered a major merger event in the redshift interval $0.0 \leq z \leq 0.5$, while by $z \sim 1$, these numbers increase to more than 90 and 55 per cent for ellipticals and spirals, respectively, indicating the lower and upper limits for the whole population of galaxies (Baugh et al. 1996). These values appear broadly consistent with the numbers derived above from our data.

As the galaxies merge, two galaxies will be replaced by one which will be on average 0.5 mag brighter from the simple coaddition of the initial luminosities, and an additional temporary star formation rate increase of a factor of ~2, triggered by the merger event. With the increase in the number of mergers at high redshifts, merger events will contribute significantly to the evolution of the luminosity function by making L^* brighter, and the number density smaller, with changing redshift. The analysis we have conducted has mainly been targeted at the most obvious merger events. We note that the number evolution and luminosity evolution that we have derived probably minimizes the full effect of mergers as the image resolution and depth of our *HST* data do not allow us to take into account mergers of smaller galaxies with bright galaxies in our sample (i.e. systems with $\delta m > 1.5$ mag).

Our results demonstrate the importance of mergers in the evolution of the luminosity function and of the luminosity density of the universe out to $z \sim 1$. The derivation of the merger fraction and of the merger rate at still higher redshifts is of great interest in order to determine the contribution of mergers to the putative peak or flattening in the UV luminosity density of the universe inferred to lie at a redshift between 1 and 2 (Madau et al. 1996).

REFERENCES

Abraham R. G., Tanvir N. R., Santiago B. X., Ellis R. S., Glazebrook K., van den Bergh S., 1996, MNRAS, 279, 47

Abraham R. G., 1998, IAU Symp. 186, Galaxy Interactions at Low and High Redshifts, in press (astro-ph/9802033)

Baugh C. M., Cole S., Frenk C. S., 1996, MNRAS, 283, 1361

Baugh C. M., Cole S., Frenk C. S., Lacey C. G., 1998, ApJ, 498, 504

Brinchmann J. et al., 1998, ApJ, in press

Broadhurst T. J., Ellis R. S., Glazebrook K., 1992, Nat, 355, 55

Carlberg R. G., Pritchet C. J., Infante L., 1994, ApJ, 435, 540

Colless M., Ellis R. S., Broadhurst T. J., Taylor K., Peterson B. A., 1993, MNRAS, 261, 19

Driver S. P., Windhorst R. A., Ostander E. J., Keel W. C., Griffiths R. E., Ratnatunga K. U., 1995, ApJ, 449, L23

Ellis R. S., Colless M., Broadhurst T. J., Heyl J. S., Glazebrook K., 1996, MNRAS, 280, 235

Fitchett M., Webster R., 1987, ApJ, 317, 653

Fomalont E. B., Windhorst R. A., Kristian J. A., Kellerman K. I., 1991, AJ, 102, 1258

Glazebrook K., Ellis R. S., Colless M., Broadhurst T. J., Allington-Smith J., Tanvir N., 1995, MNRAS, 275, L19

Glazebrook K., Ellis R. S., Santiago B., Griffiths R., 1996,

Griffiths R. E. et al., 1994, ApJ, 435, L19

Groth E. J., Kristian J. A., Lynds R., O'Neil J. Earl, Balsano R., Rhodes J., Idt W., 1994, BAAS, 185, 5309

Hammer F. et al., 1997, ApJ, 481, 49

Hernquist L., Mihos J. C., 1995, ApJ, 448, 41

Kauffmann G., 1996, MNRAS, 281, 487

Kauffmann G., White S. D. M., Guiderdoni B., 1993, MNRAS, 264, 201

Kennicutt R. C., 1996, in Friedli D., Martinod L., Pfenniger D., eds, Galaxies: Interactions and Induced Star Formation, Saas-Fee Advanced Course 26, Springer-Verlag, Berlin

Le Fèvre O., Crampton D., Hammer F., Tresse L., 1995, ApJ, 455, 60

Lee K. L., 1979, J. Am. Statistical Assoc., 74, 708

Lilly S. J., Le Fèvre O., Crampton D., Hammer F., Tresse L., 1995, ApJ, 455, 50

Lilly S. J. et al. 1998, ApJ, 500, 75

Liu C. T., Kennicutt R. C., Jr, 1995, ApJ, 450, 547

Madau P., Ferguson H. C., Dickinson M. E., Giavalisco M., Steidel C. C., Fruchter A., 1996, MNRAS, 283, 1388

Mihos J. C., 1995, ApJ, 438, L75(M95)

Mihos J. C., Hernquist L., 1994a, ApJ, 425, L13

Mihos J. C., Hernquist L., 1994b, ApJ, 431, L9

Neuschaefer L. W., Im M., Ratnatunga K. U., Griffithsm R. E., Casertano S., 1997, ApJ, 480, 59

Patton D. R., Pritchet C. J., Yee H. K. C., Ellingson E., Carlberg R. G., 1997, ApJ, 475, 29

Rocca-Volmerange B., Guiderdoni B., 1990, MNRAS, 247, 166

Schade D. J., Lilly S. J., Crampton D., Hammer F., Le Fevre O., Tresse L., 1995, ApJ, 451, L1

Schade D. J. et al., 1999, ApJ, submitted

Schweizer F., 1996, in Friedli D., Martinod L., Pfenniger D., eds, Galaxies: Interactions and Induced Star Formation, Saas-Fee Advanced Course 26, Springer-Verlag, Berlin

Woods D., Fahlman G. G., Richer H. B., 1995, ApJ, 454, 32

Yee H. K. C., Ellingson E., 1995, ApJ, 445, 37

Zepf S. E., Koo D. C., 1989, ApJ, 337, 34

This paper has been typeset from a TEX/LATEX file prepared by the author.